Available online at www.sciencedirect.com
SCIENCE DIRECT®
Journal of Nuclear Materials 323 (2003) 263–267
journal of nuclear materials
www.elsevier.com/locate/jnucmat

How fast are the ultra-fast nano-scale solid–liquid phase transitions induced by energetic particles in solids?

E.M. Lopasso [a], A. Caro [a,b,*,1], M. Caro [a,b]

[a] Centro Atómico Bariloche, 8400 Bariloche, Argentina
[b] Atomistic Simulation Group, The Queen's University Belfast, Belfast BT7 1NN, Northern Ireland

Abstract

We study the thermodynamic forces acting on the evolution of the nanoscale regions excited by collisions of energetic particles into solid targets. We analyze the role of diffusion, thermo-migration, and the liquidus–solidus two-phase field crossing, as the system cools down from the collision-induced melt under different conditions of energy deposition. To determine the relevance of these thermodynamic forces, solute redistribution is evaluated using molecular dynamics simulations of equilibrium Au–Ni solid solutions. At low collision energies, our results show that the quenching of spherical cascades is too fast to allow for solute redistribution according to equilibrium solidification as determined from the equilibrium phase diagram (zone refining effect), and only thermo-migration is observed. At higher energies instead, in the cylindrical symmetry of ion tracks, quenching rate is in a range that shows the combined effects of thermo-migration and solute redistribution that, depending on the material, can reinforce or cancel each other. These results are relevant for the interpretation of the early stage of radiation damage in alloys, and show that the combination of ultra-fast but nano-scale characteristics of these processes can still be described in terms of linear response of the perturbed system.

PACS: 61.80.Az; 66.30.−h; 82.20.Wt

1. Introduction

Energetic ions traveling in a solid lose energy via nuclear and electronic stopping. This deposited energy drives the target far from equilibrium and consequently several processes may occur: defect creation, melting and re-solidification, amorphization, disordering, mixing, etc. In situations where the nuclear stopping is the main source of energy dissipation, a ballistic phase develops into an almost spherical collision cascade, which splits into sub-cascades as energy increases [1]. At higher energies, when electronic stopping dominates, the projectile leaves behind a track of highly excited ions that decay through several possible mechanisms [2]. In addition to these spherical and cylindrical perturbations, also energy deposition in planar geometry can be studied in high-energy laser experiments in which shock and thermal waves drive the target far from equilibrium [3].

Material modifications due to such processes appear in two different time scales. In times of the order of few picoseconds, the collisional phase and the thermal spike are over, as heat is removed by electronic and ionic conduction. From there on, processes related to migration-induced nanostructural modifications, like radiation enhanced diffusion, precipitation of solutes, clustering of irradiation created point defects, etc., dominate the long-term behavior or aging of the irradiated material.

In addition to years of experimental work in this field, the last decade has introduced new knowledge from computer experiments using large-scale molecular

* Corresponding author. Address: Lawrence Livermore National Laboratory, P.O. Box 808-L-371, Livermore, CA 94551, USA. Fax: +54 2944445299.
E-mail addresses: caro2@llnl.gov, caro@cab.cnea.gov.ar (A. Caro).
[1] Leverhulme Visiting Fellow, Queen's University, Belfast.

0022-3115/$ - see front matter © 2003 Elsevier B.V. All rights reserved.
doi:10.1016/j.jnucmat.2003.08.001

dynamics and Monte Carlo simulations. Nanoscale ultra-fast features were discovered and valuable predictions were done; among them, the identification of a liquid-like structure during the thermal spike [4]. However, most of this body of research addressed cases of pure metals and ordered alloys [5]; only a few of them studied non-equilibrium solid solutions [6].

In the usual interpretation of the effects of such energetic collisions in alloys, equilibrium solid solutions are not expected to experience any modification in solute distribution, as no driving forces for such effect have so far been identified. In the early ballistic stage the atoms are displaced from their equilibrium positions creating interstitials and vacancies, and inducing ion mixing. During the thermal stage that follows, involving a liquid-like system, the temperature drop drives the system back towards solidification.

However, the presence of huge thermal gradients and the rapid quenching across the solid–liquid two phase field may provide thermodynamic forces that contribute to the solute redistribution; such forces depend on the characteristics of the system under consideration and have not yet been considered in detail.

In this paper we focus our attention on two thermodynamic forces that may give rise to solute motion: First, for a long enough lifetime of the liquid phase and strong thermal gradient, thermo-migration (Soret effect) may induce solute motion. Second, if the quenching rate is slow enough and the alloy has a significant splitting between the solidus and liquidus lines in its phase diagram, solute re-distribution on solidification across the two-phase field (zone refining) may also induce solute motion.

2. Effects on solute distribution

Thermo-migration is relevant in systems with large temperature gradients. The diffusion equation that describes this effect is written as [7]

$$\frac{\partial C_s}{\partial t} = \nabla \cdot \left[D\left(\nabla C_s + \frac{Q^* C_s}{kT^2} \nabla T \right) \right], \tag{1}$$

where C_s is the solute concentration, t is the time, D is the diffusion coefficient, Q^* is the heat of transport, k is the Boltzmann constant, and T is the temperature. The thermo-migration effect produces a solute flux whose magnitude depends on the involved time scale, the temperature gradient, and the heat of transport. The solute is driven to the cold region of the sample if Q^* is positive, and to the hot region of the sample if Q^* is negative.

The characteristics of the phase diagram also affect the solute distribution. As a solid–liquid interface is present during cooling, solute concentration in both sides of it changes as solidification proceeds. In systems with liquidus and solidus lines with negative slopes, the solute is pushed into the liquid as the solidification interface moves, resulting in a higher solute concentration in the liquid at the interface. Solidification is said to occur at equilibrium when the ratio of solute concentrations at both sides of the solid–liquid moving interface is given by the ratio of the slopes of the liquidus and solidus lines in the phase diagram, a condition that is not necessary fulfilled during the ultra-fast cooling that follows the collision. Standard results on equilibrium solidification show that the first portion of matter that solidifies has a low solute concentration, while the last solid formed is solute-enriched [8].

Depending on the particular conditions of an experiment, and on the alloy components, thermo-migration and equilibrium solidification may cancel or reinforce each other, according the sign of Q^* and the slope of the lines in the phase diagram.

3. Properties of Au–Ni dilute alloys

A computational study of these effects requires a large number of atoms; therefore simple empirical potentials have to be used to describe the atomic interactions. A proper knowledge of the equilibrium and non-equilibrium thermodynamics implicit in the model potential is required. In a previous work we determined the heat of transport and diffusion coefficients in dilute liquid Au–Ni alloys [9] described by an embedded atom type potential [10]. We measured Q^* through MD simulations for both Au and Ni acting as solute into each other, and found that Au as a solute in Ni has a tendency to move towards the cold region of the sample, while Ni as a solute in Au has the opposite tendency.

With respect to the Au–Ni phase diagram, Fig. 1 represents the calculated liquidus, solidus, and solvus lines for the EAM potentials used in MD calculations,

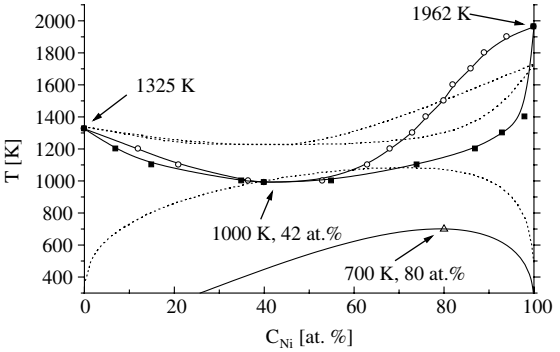

Fig. 1. Experimental (dotted) and calculated Au–Ni phase diagram. See Ref. [11].

as we recently determined [11]. The dotted lines are the experimental data [12]. Though there are quantitative differences, the two-phase fields in both cases show a broad splitting in the Ni-rich region, and a narrow one in the Au-rich region; additionally, both dilute solid solutions show negative slopes in the solidus and liquidus lines. From the phase diagram predicted by the model we then expect that equilibrium solidification would significantly increase the solute distribution in the core of a thermal spike for the Ni-rich region of the phase diagram (large s–l splitting), while the Au-rich solutions would slightly be affected by this effect (small splitting). Additionally, thermo-migration will enhance solute concentration in the liquid if Ni is the solute (negative Q^*), while the contrary will happen if Au is the solute. Consequently these two driving forces would reinforce each other in the Au-rich solutions, while they would show a tendency to cancel each other in the Ni-rich solutions.

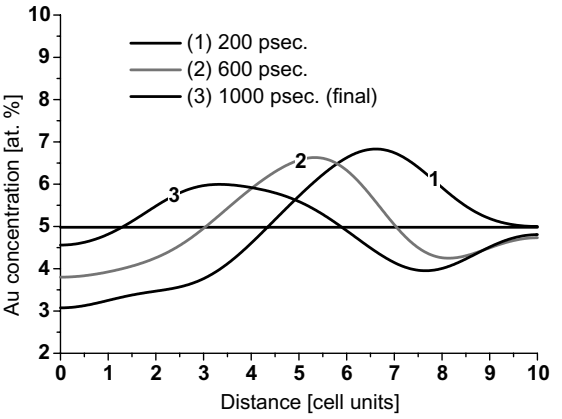

Fig. 2. Au concentration in $Ni_{95}Au_5$ in a MD simulation of a one-dimensional thermal gradient with slow cooling rate.

4. Results

We simulated irradiation experiments that induce distinct geometry of the excited regions, with different surface to volume ratios of the liquid zones (different quenching rates and interface velocities), namely: spherical cascades (3-D) for low energy ions, cylindrical tracks (2-D) for high-energy ions, and planar laser shots (1-D). In this work we report a 1-D and a 2-D geometries, both in $Ni_{95}Au_5$ solid solutions.

To determine the relative importance of the two driving forces under consideration, we analyze the simple 1-D geometry of a linear T-gradient, and perform both a MD simulation and an analytic calculation. A variable linear thermal gradient was imposed to a $20\times8\times8$ cells sample, with temperature control at both ends (cold ends), and at the center (hot center). Periodic boundary conditions in 3-D and constant volume were used in the simulations. The cold ends were kept at 1000 K, while the hot center was initially set at 11 000 K and then cooled at constant speed down to 1000 K. The constant cooling of the hot center gives a variable solid–liquid interface speed, as the temperature gradient is linear. A fast cooling of 500 K/ps, and a slow cooling of 10 K/ps, were simulated.

The evolution of the concentration at three different times (early, intermediate, final) in the MD calculation for the slow cooling case is shown in Fig. 2. The thermo-migration effect is clearly seen at the early times of the run, showing solute depletion at the center. At later stages, the solute is pushed to the hot center of the sample by the solid–liquid interface, in opposition to the thermo-migration effect. At the end of the run the concentration profile shows a peak that moved from the cold to the hot region, clearly indicating a competition between the two driving forces at this quenching rate, namely, the solute re-distribution during solidification is seen, indicating some degree of equilibrium solidification. The fast cooling case, not reported here, shows no significant changes in concentration, indicating that the equilibrium solidification does not take place.

To interpret the MD results, we compare them with the analytic solution of 1-D solidification as it appears in textbooks. We shall not discuss details of the equations here, we refer the reader to [13]; we just highlight the fact that the analytic solution assumes first equilibrium solidification, that is, the ratio of solute concentration at both sides of the solid–liquid moving interface is forced to be equal to the ratio of the slopes of the solidus–liquidus lines in the phase diagram, and second it assumes diffusion in the liquid phase. Additionally, the model includes thermo-migration in the diffusion equation that controls solute motion in the liquid (see Eq. (1)). The differential equation is solved numerically as cooling proceeds at both the same slow and fast rates as in the MD simulations. The final concentration profiles are shown in Fig. 3. In the fast cooling case, a large solute peak at the center of the sample reflects a huge 'zone refining' effect. This peak is absent in the MD simulation, indicating that the assumption of equilibrium solidification, which leads to the profile of Fig. 3, is not what really happens in the MD simulations. Conversely, the concentration profile for the slow cooling case is very similar to the MD result: a solute depletion at the boundary of the liquid zone, and a solute peak close to – but not at – the center of the sample (see curve 3, Fig. 2). The results of the analytic equations help us confirming the interpretation given above in the sense that fast cooling only shows the effects of thermo-migration, while slow cooling show both, thermo-migration, and zone refining.

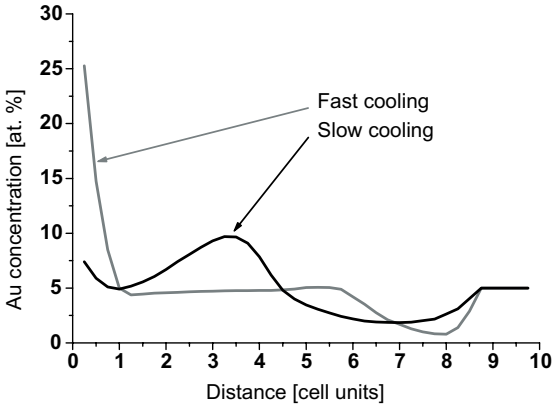

Fig. 3. Concentration profiles predicted by the analytic calculation for slow and fast cooling rates in $Ni_{95}Au_5$.

From these 1-D results we can conclude that the fast cooling rate, showing differences between the analytic solution and MD, implies that equilibrium solidification is not reached in the MD simulation. In contrast, the slow cooling rate shows similar qualitative behavior in analytic and MD results, indicating some degree of equilibrium in the MD calculation.

There are differences in the concentration values in the MD simulation and the analytic calculation for the slow cooling; they are due to the strong assumption of equilibrium solidification in the analytic solution, which is taken as an extreme case, while MD reflects the real behavior of the model system, somewhere between complete equilibrium and no re-distribution at all.

For the 2-D symmetry, the track case, we use a sample of $64\times64\times16$ unit cells in the x–y–z directions, at 300 K. The collision leaving a track along the z-axis was simulated by imposing a Gaussian temperature distribution with $\sigma = 2a_0$, at the x–y center of the sample, with cylindrical symmetry in the z-direction. The deposited energy represents 400 eV/Å, which is in the range usually attainable by swift heavy ions [2]. After the initial energy deposition, heat is removed by a thermostat set at 300 K, acting on the lateral boundaries of the sample. As a result, during the first few picoseconds the liquid interface moves from the center outwards, expanding the volume of the melt, which reaches a maximum, shown in Fig. 4, and with a temperature at the center of approximately 11 000 K. The system cools below the melting temperature after about 20 ps, recovering the crystalline state. Since the center of the sample cools down from 11 000 to 1000 K in about 20 ps, the average cooling rate is ~500 K/ps, the average interface speed is ~2 Å/ps, and the initial thermal gradient is ~1000 K/Å. With a heat of transport of the order of 0.5 eV, a thermal gradient of this magnitude induces a

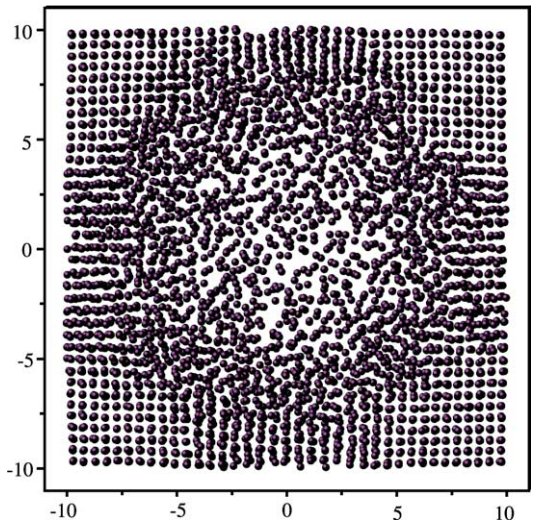

Fig. 4. $Ni_{95}Au_5$ sample after 1 ps from the energy deposition. Distances in cell units.

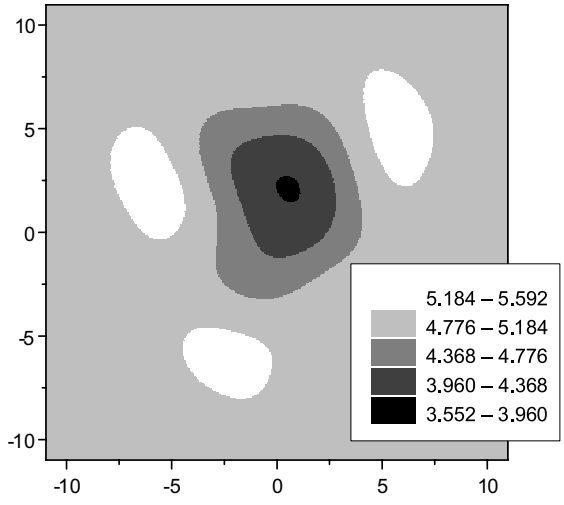

Fig. 5. Final concentration of Au as a solute in $Ni_{95}Au_5$ after an event of energy deposition with cylindrical symmetry (track event). Distances in cell units.

force of ~0.1 eV/Å, large enough to produce measurable effects.

The final solute concentration is shown in Fig. 5. The solute moved away from the center of the sample, which reflects a dominance of thermo-migration over solute redistribution upon re-solidification. From this simulation it is not possible to separate the contribution of the two effects, namely, thermo-migration and solute redis-

tribution. What is clear though is that the former dominates the outcome of a 400 eV/Å track in $Ni_{95}Au_5$.

5. Discussion

The 1-D results shown help us in the interpretation of the track simulation: the fast cooling observed after the track is too fast for a manifestation of the equilibrium solidification. The average speed of the interfaces during the track and the fast cooling under the 1-D temperature gradient were estimated to be 2 Å/ps, while in the slow cooling it was about 0.04 Å/ps. These values provide us with two boundaries for the interface speed: at 0.04 Å/ps and below, equilibrium solidification is clearly operative; at 2 Å/ps and above, its effects cannot be appreciated in the simulations. In terms of the speed of sound c, these boundaries are approximately 10^{-3} c and 10^{-1} c. These results from MD are in excellent agreement with the qualitative analysis given in [13] which runs as follows: in the liquid the average inter-particle distance a is $\sim$2 Å, and the diffusion coefficient D at 2000 K is $\sim$0.6 Å^2/ps, therefore, the order of magnitude of a velocity associated to diffusing atoms is $v_{\text{limit}} = D/a \sim 0.2$ Å/ps; consequently if the solidifying interface moves faster than v_{limit}, solute atoms can not follow and solute trapping, as opposed to equilibrium solidification (zone refining), appears. Our simulations tested interface velocities one order of magnitude above and below this limit and the results are in full agreement with this interpretation.

A similar track was also simulated in the $Au_{95}Ni_5$ system. Only the thermo-migration effect is observed at the initial stages of cooling, enriching the core of the track because in this case the heat of transport is negative. As the equilibrium phase diagram shows no splitting between solidus and liquidus, no zone refining is observed.

6. Conclusions

The MD simulations of tracks and 1-D thermal gradients in equilibrium solid solutions as reported here, give us quantitative proofs of the existence of these two thermodynamic forces affecting solute redistribution in these ultra-fast nano-scale phase transitions. We can conclude that a clear distinction can be made between three regimes: (i) collision events dominated by nuclear stopping power (producing essentially spherical cascades and sub-cascades, with solid–liquid interface velocities faster than 1 Å/ps) show thermo-migration if the heat of transport is of the order of 0.5 eV or larger, and solute trapping; (ii) collisions with energies in the electronic stopping power regime (producing cylindrical tracks with slower cooling rates) are in the frontier of the reinforcement or cancellation between thermo-migration and solute re-distribution; and (iii) laser shots (producing one-dimensional perturbation fronts with the slowest cooling rate) where both effects reported here should clearly be observable.

Additionally, this study also shows the importance of a proper knowledge of the thermodynamic properties implicit in the empirical models, if they are intended to describe alloys under irradiation. Although far from equilibrium, the formalism of the heat of transport based on linear response and Onsager relations [14] proves to give a reasonable quantitative framework to interpret the results of MD simulations.

Acknowledgements

Authors acknowledge fruitful discussion with R. Passianot. M.C. and A.C. gratefully acknowledge the Leverhulme Trust for financial support. This work was partially supported by Conicet PIP 4205/96, PIP 0664/98.

References

[1] T. Diaz de la Rubia, R.S. Averback, R. Benedek, W.E. King, Phys. Rev. Lett. 59 (1987) 1930.
[2] A. Dunlop, H. Dammak, D. Lesueur, Nucl. Instrum. and Meth. B 112 (1996) 23.
[3] V. Schmidt, W. Husunski, G. Betz, Phys. Rev. Lett. 85 (2000) 3516.
[4] R.S. Averback, T. Diaz de la Rubia, in: H. Ehrenreich, F. Spaepen (Eds.), Solid State Physics, vol. 51, Academic Press, NY, 1998, p. 281.
[5] G. Martin, P. Bellon, in: H. Ehrenreich, F. Spaepen (Eds.), Solid State Physics, vol. 50, Academic Press, NY, 1996, p. 189.
[6] T.J. Colla, H.M. Urbassek, K. Nordlund, R.S. Averback, Phys. Rev. B 63 (2001) 104206/1-7.
[7] J.P. Stark, Solid State Diffusion, John Wiley, 1976, p. 124.
[8] D.A. Porter, K.E. Easterling, Phase Transformations in Metals and Alloys, 2nd Ed., Chapman and Hall, London, 1992, p. 208.
[9] E.M. Lopasso, M. Caro, A. Caro, Phys. Rev. B 63 (2001) 174105.
[10] S.M. Foiles, M.I. Baskes, M.S. Daw, Phys. Rev. B 33 (1986) 7983.
[11] E. Ogando Arregui, M. Caro, A. Caro, Phys. Rev. B 66 (2002) 054201.
[12] W.W. Scott Jr., in: T.B. Massalski (Ed.), Binary Alloy Phase Diagrams, 2nd Ed., ASM International, 1992, p. 402.
[13] J.M. Howe, Interfaces in Materials, John Wiley, 1997.
[14] L. Onsager, Phys. Rev. 38 (1931) 2265.